Chargino Contributions in $B \to \phi K_S$ CP Asymmetry

Yili Wang
Department of Physics and Astronomy, Iowa State University, Ames, Iowa 50011, USA.
(February 1, 2008)

Abstract

CP asymmetry in $B \to \phi K_S$ decay is studied in the special context of supersymmetry theories, in which the charginos play an important role. We find that in addition to the gluino, the chargino can also make large contributions to CP asymmetry in $B \to \phi K_S$ decay. After considering the constraints from $B \to J/\psi K_S$ decay, we study three special scenarios: (a). Large mixing between left-handed charm and top squarks(LL mixing); (b). Large mixing between right-handed charm and top squarks (RR mixing); (c). Large mixing between both left-handed charm-top squark and right-handed charm-top squark(LL+RR mixing). We show quantitatively that because of large squark mixing within the second and third generations, an $\mathcal{O}(1)$ effect on CP violation in $B \to \phi K_S$ is possible.

PACS numbers: 13.25.Hw; 12.60.Jv; 11.30.Pb

I. INTRODUCTION

In standard model, all the CP asymmetries in the B system can be accounted for with a single phase in Cabbibo-Kobayashi-Maskawa mixing matrix [1]. It predicts that the time dependent CP asymmetry in $B \to \phi K_S$ decay is the same as the CP asymmetry in $B \to J/\psi K_S$ decay. That is:

$$S_{J/\psi K_S} = S_{\phi K_S} = sin2\beta = 0.731 \pm 0.056(SM)$$

Any difference between these two decays would be evidence of new physics beyond the standard model. Finding CP violation in the B system is a very important goal in B factories.

BaBar [2] and Belle [3] measurements on CP asymmetries in $B \to J/\psi K_S$ decay have provided the first evidence for CP violation in the B system.

$$\begin{array}{rcl} sin2\beta(B \to J/\psi K_S) & = & 0.741 \pm 0.067 \pm 0.033 \ \ (BaBar) \\ sin2\beta(B \to J/\psi K_S) & = & 0.733 \pm 0.057 \pm 0.028 \quad (Belle) \end{array} \tag{1}$$

The average of their results is:

$$S_{J/\psi K_S} = sin2\beta = 0.734 \pm 0.054,$$

This result is in good agreement with the SM prediction [4]. Therefore, we can conclude that CP is significantly violated and the CKM phase angle is the dominant source of CP violation.

However, the CKM mechanism is challenged by the recent measurements of the BaBar and Belle collaborations in $B \to \phi K_S$ decay.

$$\begin{array}{rcl} sin2\beta(B \to \phi K_S) & = & +0.45 \pm 0.43 \pm 0.07 \ \ (BaBar) \\ sin2\beta(B \to \phi K_S) & = & -0.96 \pm 0.50^{+0.09}_{-0.11} \quad (Belle) \end{array} \tag{2}$$

The average of these two measurements implies:

$$S_{\phi K_S} = sin2\beta = -0.15 \pm 0.33.$$

which deviates from the SM prediction by 2.7σ. The 2σ difference between $S_{J/\psi k_S}$ and $S_{\phi K_S}$ is expected to be an indication of new physics. Many papers have explored potential new physics contributions [5–9] to $B \to \phi K_S$ decay. Among them, supersymmetry is one of the most significant candidates to account for this 2σ deviation.

In $B \to J/\psi K_S$ decay, standard model contributions dominate the tree level diagrams and any new physics enters only in loop diagrams, which are suppressed naturally. As a result, in order to have a significant supersymmetric contribution, a large SUSY CP violating phase is required. Such large phases usually do not exist in most of the supersymmetric models. Therefore the CP asymmetry in $S_{J/\psi K_S}$ is dominated by the standard model contribution. Unlike the case of $B \to J/\psi K_S$, there are no tree level diagrams in $B \to \phi K_S$ decay because $b \to s\bar{s}s$, the dominant process in $B \to \phi K_S$, is induced only at one loop level in the standard model. Both SM and SUSY contributions appear at one loop level. Thus

SUSY contributions are more significant in $B \to \phi K_S$ decay and are expected to explain the 2σ difference.

SUSY contributions to $B \to \phi K_S$ decay come mainly from penguin and box diagrams containing gluino, chargino and neutralino loops. The contributions from neutralino loops are much smaller than the contributions from gluino and chargino loops. We ignore contributions from neutralinos in our computation. There are several papers investigating on SUSY contributions to $B \to \phi K_S$ decay [10–18], especially the gluino loop contributions [19–24]. Only a few include the chargino diagrams, which can also affect the result substantially [25]. The main purpose of this paper is to study chargino contributions to the CP asymmetry in $B \to \phi K_S$ decay. The chargino contributions depend on the details of the model. However, we try to be as general as possible in our analysis. To emphasize the chargino loop contributions, we work in a special basis where the down-type squark mass matrix is diagonalized. There is no intergeneration mixing in the down-type squark sector. In this scenario, gluino contributions to $B \to \phi K_S$ decay are ruled out and chargino contributions are the dominant contributions.

This paper is organized as follows: In the next section, we present the formula for CP violation in the B system and introduce the effective field theory for the $b \to s$ transition. Section III is devoted to the discussion of supersymmetric contributions to the CP asymmetry in $B \to \phi K_S$ process. Section IV includes the conclusion and the loop functions are showed in Appendix.

II. CP VIOLATION IN $B \to \phi K_S$ DECAY

In the B system, the time dependent CP asymmetry in $B \to \phi K_S$ decay is defined as

$$A_{\phi K_S}(t) = \frac{\Gamma(\overline{B}^0(t) \to \phi K_S) - \Gamma(B^0(t) \to \phi K_S)}{\Gamma(\overline{B}^0(t) \to \phi K_S) + \Gamma(B^0(t) \to \phi K_S)}$$

$$= C_{\phi K_S} \cos \Delta M_{B_d} t + S_{\phi K_S} \sin \Delta M_{B_d} t \tag{3}$$

where ΔM_{B_d} is the mass difference between the two neutral B mesons. $C_{\phi K_S}$ and $S_{\phi K_S}$ are

$$C_{\phi K_S} = \frac{|\lambda(\phi K_S)|^2 - 1}{|\lambda(\phi K_S)|^2 + 1}, \quad S_{\phi K_S} = \frac{2Im\left[\frac{q}{p}\,\lambda(\phi K_S)\right]}{|\lambda(\phi K_S)|^2 + 1}. \tag{4}$$

p and q are the mixing parameters defined as:

$$|B_\pm> = p|B^0> \pm q|\bar{B}^0>$$

$\lambda_{\phi K_S}$ is a ratio of decay amplitudes:

$$\lambda_{\phi K_S} = \frac{\overline{A}(\overline{B}^0 \to \phi K_S)}{A(B^0 \to \phi K_S)} \tag{5}$$

From above formulae, we notice that there are two sources of CP violation [26]. One is from the mixing $|\frac{q}{p}| \neq 1$, the other is from the ratio of decay amplitudes $|\frac{\overline{A}}{A}| \neq 1$ [4,27]. In

the SM, loop diagrams with W boson and top quark dominate the $b \to sss$ decay channel. In this channel, $\lambda_{\phi K_S} = \frac{\overline{A}^{SM}(\overline{B}^0 \to \phi K_S)}{A^{SM}(B^0 \to \phi K_S)} = \frac{V_{tb}V_{ts}^*}{V_{tb}^*V_{ts}} = 1$. There is no CP violation from the ratio of decay amplitudes. Thus, CP asymmetry in $B \to \phi K_S$ decay comes mainly from mixing , which is the same with $B \to J/\psi K_S$ decay.

Supersymmetry can contribute to mixing, $\Delta B = 2$ transitions, and to decay $\Delta B = 1$ transitions. SUSY contributions to the decay amplitudes are through penguin and box diagrams [28], while contributions to the mixing parameters are only through box diagrams. To concentrate on the chargino contributions, we choose a basis, in which the down-type squark mass is diagonalized. There is no intergeneration mixing for down-type sector. The gluino contributions are ruled out by the choice of basis. SUSY contributions are mainly chargino contributions.

The effective Hamiltonian in $\Delta B = 1$ transitions is:

$$H = \sum_{i=1}^{6} [C_i(\mu)\mathcal{O}_i(\mu)] + C_g\mathcal{O}_g \tag{6}$$

As in Ref. [23,29], the operators we choose are:

$$\begin{aligned}
\mathcal{O}_1 &= (\bar{s}_\alpha\gamma_\mu P_L c_\beta)(\bar{c}_\beta\gamma^\mu P_L b_\alpha),\\
\mathcal{O}_2 &= (\bar{s}_\alpha\gamma_\mu P_L c_\alpha)(\bar{c}_\beta\gamma^\mu P_L b_\beta),\\
\mathcal{O}_3 &= (\bar{s}_\alpha\gamma_\mu P_L b_\alpha)(\bar{s}_\beta\gamma^\mu P_L s_\beta),\\
\mathcal{O}_4 &= (\bar{s}_\alpha\gamma_\mu P_L b_\beta)(\bar{s}_\beta\gamma^\mu P_L s_\alpha),\\
\mathcal{O}_5 &= (\bar{s}_\alpha\gamma_\mu P_L b_\alpha)(\bar{s}_\beta\gamma^\mu P_R s_\beta),\\
\mathcal{O}_6 &= (\bar{s}_\alpha\gamma_\mu P_L b_\beta)(\bar{s}_\beta\gamma^\mu P_R s_\alpha),\\
\mathcal{O}_g &= \frac{g_s}{8\pi^2} m_b(\bar{s}_\alpha T^a_{\alpha\beta}\sigma_{\mu\nu}P_R b_\beta)G^{a\mu\nu}
\end{aligned} \tag{7}$$

where α and β are color indices, $P_L = (1-\gamma_5)/2$, and $\sigma_{\mu\nu} = \frac{i}{2}[\gamma^\mu, \gamma^\nu]$. The contribution from the operator $\mathcal{O}_\gamma = \frac{e}{8\pi^2} m_b(\bar{s}_\alpha\sigma_{\mu\nu}P_R b_\alpha)F^{\mu\nu}$ is very small and is ignored in this paper. Operators proportional to s-quark mass m_s are also ignored because of the small s-quark mass.

In the SM, the Wilson coefficients $C_{3\sim6}$ in $B \to \phi K_S$ decay have been computed to NLL order, and C_g has been computed to LL order. The values we used are in ref. [30].

In SUSY, up-squark masses are taken to be non-degenerate. We use the mass eigenbasis in the computation. There are large mixing between the second and third generations in up-type sector. The mass matrix takes the form:

$$\tilde{m}^2_{\tilde{u}} = \begin{pmatrix}
\tilde{m}^2_{Lu} & 0 & 0 & 0 & 0 & 0\\
0 & \tilde{m}^2_{Lc} & \tilde{m}^2_{Lct} & 0 & 0 & 0\\
0 & \tilde{m}^{*2}_{Lct} & \tilde{m}^2_{Lt} & 0 & 0 & m_t A_t cot\beta\\
0 & 0 & 0 & \tilde{m}^2_{Ru} & 0 & 0\\
0 & 0 & 0 & 0 & \tilde{m}^2_{Rc} & \tilde{m}^2_{Rct}\\
0 & 0 & m_t A_t cot\beta & 0 & \tilde{m}^{*2}_{Rct} & \tilde{m}^2_{Rt}
\end{pmatrix}. \tag{8}$$

This mass matrix can be diagonalized by a unitary matrix $R_{\tilde{u}}$. That is:

$$R^+_{\tilde{u}}\tilde{m}^2_{\tilde{u}}R_{\tilde{u}} = diag(\tilde{m}^2_{L1}, \tilde{m}^2_{L2}, \tilde{m}^2_{L3}, \tilde{m}^2_{R1}, \tilde{m}^2_{R2}, \tilde{m}^2_{R3}),$$

It is useful to define the 6×3 matrices such that

$$(\Gamma^{q_L})_{ai} = (R_{\tilde{u}})_{ai}, \quad (\Gamma^{q_R})_{ai} = (R_{\tilde{u}})_{ai+3}.$$

where a = 1, ... ,6 denotes the mass eigenstates and i = u,c,t labels the gauge eigenstates.

The chargino mass matrix is

$$\tilde{M}_{\tilde{\chi}^{\pm}} = \begin{pmatrix} M_2 & \sqrt{2}M_W sin\beta \\ \sqrt{2}M_W cos\beta & \mu \end{pmatrix}. \tag{9}$$

where we assume the mass of the W-ino field, M_2, is real and positive. The non observation of the neutron electric dipole moment (EDM) strongly constrains the phase of μ. A non-zero phase of μ does not significantly affect our results, we keep the phase of μ to be zero for sake of simplicity.

The chargino mass matrix can be diagonalized by a biunitary transformation

$$diag(m_{\tilde{\chi}_1^{\pm}}, m_{\tilde{\chi}_2^{\pm}}) = U\tilde{M}_{\tilde{\chi}^{\pm}}V^T$$

where U and V are unitary matrices defined as

$$U = \begin{pmatrix} cos\theta_U & sin\theta_U \\ -sin\theta_U & cos\theta_U \end{pmatrix}. \tag{10}$$

$$V = \begin{pmatrix} cos\theta_V & sin\theta_V \\ -sin\theta_V & cos\theta_V \end{pmatrix}. \tag{11}$$

with mixing angles [29]

$$\begin{aligned} \sin 2\theta_{U,V} &= \frac{2M_W[M_2^2 + \mu^2 \pm (M_2^2 - \mu^2)\cos 2\beta + 2\mu M_2 \sin 2\beta]^{1/2}}{m^2_{\tilde{\chi}_1^{\pm}} - m^2_{\tilde{\chi}_2^{\pm}}}, \\ \cos 2\theta_{U,V} &= \frac{M_2^2 - \mu^2 \mp 2M_W^2 \cos 2\beta}{m^2_{\tilde{\chi}_1^{\pm}} - m^2_{\tilde{\chi}_2^{\pm}}}. \end{aligned} \tag{12}$$

We calculated Wilson coefficients of SUSY diagrams in Fig. 1 with chargino loops [23,31–33].

$$\begin{aligned} C_3^{SUSY} = \sum_{i,h,j,k} & -\frac{\alpha_w^2}{4m^2_{\tilde{\chi}_j}}(G^{*iks}_{u_L} - H^{*iks}_{u_R})(G^{ihs}_{u_L} - H^{ihs}_{u_R})(G^{*jhs}_{u_L} - H^{*jhs}_{u_R})(G^{jkb}_{u_L} - H^{jkb}_{u_R}) \\ & G(x_{m_{\tilde{u}_k}, m_{\tilde{x}_j}}, x_{m_{\tilde{u}_k}, m_{\tilde{x}_j}}, x_{m_{\tilde{u}_k}, m_{\tilde{x}_j}}) \\ & + \sum_{j,k} \frac{\alpha_s \alpha_w}{6m^2_{\tilde{\chi}_j}}(G^{*jks}_{u_L} - H^{*jks}_{u_R})(G^{*jkb}_{u_L} - H^{*jkb}_{u_R})C_1(x_{m_{\tilde{u}_k}, m_{\tilde{x}_j}}) \\ & + \sum_{j,k} \frac{2\alpha_w \alpha_1}{9m^2_{\tilde{\chi}_j}}(G^{*jks}_{u_L} - H^{*jks}_{u_R})(G^{*jkb}_{u_L} - H^{*jkb}_{u_R}) \\ & \Big(-C_1(x_{m_{\tilde{u}_k}, m_{\tilde{x}_j}}) + C_2(x_{m_{\tilde{u}_k}, m_{\tilde{x}_j}})\Big) \end{aligned}$$

$$
\begin{aligned}
C_4^{SUSY} &= \sum_{j,k} -\frac{\alpha_s\alpha_w}{2m^2_{\tilde{\chi}_j}}(G^{*jks}_{u_L} - H^{*jks}_{u_R})(G^{*jkb}_{u_L} - H^{*jkb}_{u_R})C_1(x_{m_{\tilde{u}_k},m_{\tilde{x}_j}}) \\
C_5^{SUSY} &= \sum_{i,h,j,k} \frac{\alpha_w^2}{2m^2_{\tilde{\chi}_j}}(G^{*iks}_{u_L} - H^{*iks}_{u_R})H^{ihs}_{u_L}H^{*jhs}_{u_L}(G^{jkb}_{u_L} - H^{jkb}_{u_R}) \\
&\quad x_{m_{\tilde{\chi}_i},m_{\tilde{x}_j}} G_1(x_{m_{\tilde{u}_k},m_{\tilde{x}_j}}, x_{m_{\tilde{u}_k},m_{\tilde{x}_j}}, x_{m_{\tilde{u}_k},m_{\tilde{x}_j}}) \\
&\quad + \sum_{j,k} \frac{\alpha_s\alpha_w}{6m^2_{\tilde{\chi}_j}}(G^{*jks}_{u_L} - H^{*jks}_{u_R})(G^{*jkb}_{u_L} - H^{*jkb}_{u_R})C_1(x_{m_{\tilde{u}_k},m_{\tilde{x}_j}}) \\
&\quad + \sum_{j,k} \frac{2\alpha_w\alpha_1}{9m^2_{\tilde{\chi}_j}}(G^{*jks}_{u_L} - H^{*jks}_{u_R})(G^{*jkb}_{u_L} - H^{*jkb}_{u_R}) \\
&\quad \Big(-C_1(x_{m_{\tilde{u}_k},m_{\tilde{x}_j}}) + C_2(x_{m_{\tilde{u}_k},m_{\tilde{x}_j}})\Big) \\
C_6^{SUSY} &= \sum_{j,k} -\frac{\alpha_s\alpha_w}{2m^2_{\tilde{\chi}_j}}(G^{*jks}_{u_L} - H^{*jks}_{u_R})(G^{*jkb}_{u_L} - H^{*jkb}_{u_R})C_1(x_{m_{\tilde{u}_k},m_{\tilde{x}_j}}) \\
C_g^{SUSY} &= \sum_{j,k} \frac{\alpha_w\pi}{2m^2_{\tilde{\chi}_j}}(G^{*jks}_{u_L} - H^{*jks}_{u_R})(G^{*jkb}_{u_L} - H^{*jkb}_{u_R})D_1(x_{m_{\tilde{u}_k},m_{\tilde{x}_j}}) \\
&\quad + \sum_{j,k} \frac{\alpha\pi}{2m^2_{\tilde{\chi}_j}}(G^{*jks}_{u_L} - H^{*jks}_{u_R})H^{*jkb}_{u_R}\frac{m_{\tilde{\chi}_j}}{m_b}D_2(x_{m_{\tilde{u}_k},m_{\tilde{x}_j}}) \qquad (13) \\
& \qquad (14)
\end{aligned}
$$

where

$$
G^{jki}_{u_L} = V^*_{j1}(\Gamma_{u_L}V_{CKM})^{ki}, \qquad H^{jki}_{U_R} = V^*_{j2}(\Gamma_{U_R}V_{CKM})^{ki}\frac{M_U}{\sqrt{2}M_w sin\beta} \qquad (15)
$$

$m_{\tilde{\chi}_j}$, $j = 1, 2$ are chargino masses, and $x_{m_A,m_B} = m_A^2/m_B^2$. The loop functions are given in Appendix.

In addition to Wilson coefficients, the hadronic matrix elements of the operators are also needed in computing the SUSY contributions to the CP asymmetry in $B \to \phi K_S$ decay. We use the results in ref. [23,34]

$$
\begin{aligned}
\langle\phi K_S|\mathcal{O}_{3,4}|\bar{B}^0_d\rangle &= \frac{1}{4}H\left(1 + \frac{1}{N_c}\right) \\
\langle\phi K_S|\mathcal{O}_5|\bar{B}^0_d\rangle &= \frac{1}{4}H \\
\langle\phi K_S|\mathcal{O}_6|\bar{B}^0_d\rangle &= \frac{1}{4}H\frac{1}{N_c} \\
\langle\phi K_S|\mathcal{O}_g|\bar{B}^0_d\rangle &= \kappa\frac{\alpha_s}{2\pi}H\frac{N_c^2 - 1}{2N_c^2}. \qquad (16) \\
& \qquad (17)
\end{aligned}
$$

where the analytical expression for H is in Appendix B of ref. [23]. The value of κ is approximately -1.1 [20,23].

III. NUMERICAL RESULTS

With the formulae in section II, we can numerically analyze the chargino contributions in B system. There are three kinds of mixing in the up-squark mass matrix: Left-Left, Right-Right and Left-Right. Each mixing contributes a mixing angle and a phase angle in $S_{\phi K_S}$ computation. However, the phase of μ is strongly constrained by the neutron electric dipole moment (EDM). We have checked that our results have no substantially dependence on μ. To simplify our computation, we take the phase of μ to be zero in this paper.

The agreement between the CP asymmetry in $B \to J/\psi K_S$ decay observed by BaBar and Belle with the SM prediction leaves very little room for new physics contributions in $S_{J/\psi K_S}$. It strongly constrains the SUSY contributions to $S_{J/\psi K_S}$ and strongly suppresses the CP violating phase in $B \to \phi K_S$ system [35], which will be noticed in the following analysis.

In order to simplify the analysis, we consider three special cases. First, left-left mixing dominates, LL scenario. Right-right mixing is very small and can be ignored in this scenario. The second scenario is right-right mixing dominant, RR scenario, while the last one has comparable left-left and right-right mixing contributions, LL + RR scenario. We need to consider both contributions in the last case. Because of the large parameter space, we only show some results for RR + LL scenario with specific simplifications.

A. Left-Left Mixing Dominant

In this scenario, left-left mixing is the only sizable mixing and there is only one phase and one mixing angle. We take the mixing matrix to be:

$$R = \begin{pmatrix} cos\theta_{23} & sin\theta_{23}e^{i\phi_L} \\ -sin\theta_{23} & cos\theta_{23}e^{-i\phi_L} \end{pmatrix}. \tag{18}$$

where θ_{23} is the mixing angle. The subscript 23 represents the left-left mixing and is the mixing between second and third rows in up-squark mass matrix. ϕ_L is the phase angle. We expect that these mixing and phase angles can significantly alter the value of $S_{\phi K}$. We have checked that the precise values of M_2 and μ do not have a substantial effect on our results. We use a range of values of M_2 and μ from 2 GeV to about 400 GeV. We obtain almost the same results. Thus, we take M_2 and μ to be 200 GeV in most of our calculations.

In this scenario, we have parameters

$$m_{\tilde{L}_2}, m_{\tilde{L}_3}, m_{\tilde{\chi}_2}, m_{\tilde{\chi}_1}, tan\beta, \theta_{23}, \phi_L.$$

with $m_{\tilde{L}_3} < m_{\tilde{L}_2}$ and $m_{\tilde{\chi}_1} < m_{\tilde{\chi}_2}$. As pointed in ref. [35], the imaginary parts of this matrix are stringently constrained by $B \to J/\psi K_S$ decay. In order for the mixing angle θ_{23} to be less constrained, the phase ϕ_L we use in our computation is very severe constrained, $\phi_L \leq 10^{-2}$.

There are seven parameters. Their effects on $S_{\phi K_S}$ are different. In Fig. 2, we plot $S_{\phi K}$ as a function of $m_{\tilde{L}_3}$ and $m_{\tilde{\chi}_1}$ within the range $-0.7 < S_{\phi K} < 0.7$. We fixed $tan\beta = 5$, and $m_{\tilde{L}_2} = 5$ TeV. θ_{23} is taken to be $\pi/4$, and $\phi_L = 0.01$. In frame (a), The value of κ is equal to -1.1 and $m_{\tilde{\chi}_2} = 10 m_{\tilde{\chi}_1}$. In frame (b), κ has the same value as in frame (a), but $m_{\tilde{\chi}_2} = 100 m_{\tilde{\chi}_1}$. We change κ to -2 in frame (c) and frame (d) with $m_{\tilde{\chi}_2} = 10 m_{\tilde{\chi}_2}$ in frame

(c) and $m_{\tilde{\chi}_2} = 100 m_{\tilde{\chi}_2}$ in frame (d). Within the shaded region, $S_{\phi K}$ is larger than -0.7, but smaller than 0.7. From this graph, we notice that:

- There are many assumptions in the process of κ estimation. $\kappa = -1.1$ is just an approximate value. We present results for different values of κ to show the dependence of $S_{\phi K_S}$ on κ. The main SUSY contributions in this scenario come from penguin diagrams. The hadronic matrix of the corresponding operator is proportional to κ and κ surely has some effect on $S_{\phi K_S}$. This can be observed through the difference among graphs in Fig. 2.

- We show how large the effect of the parameter κ is. We take κ to be -2 in frame (c) and frame (d). Except for these two frames, κ is fixed to -1.1 in all other graphs.

- We focus on chargino loop contributions. Any changes in the chargino parameters have a large influence on our results. As is seen in frame (c) and frame (d), increasing $m_{\tilde{\chi}_2}$ changes the allowed values significantly.

- There are big gaps around the line $m_{\tilde{L}_3} = m_{\tilde{\chi}_1}$. We refer the reader to the loop functions in Eq. 14, which are presented explicitly in Appendix. When the chargino and squark masses are equal, the functions in the Appendix take a different form and cause the big gaps in the graphs.

- The small discontinuity in frame (a) and frame (b) at $m_{\tilde{\chi}_1} = 500$ GeV arises for the same reason. That is because $m_{\tilde{\chi}_2}$ is ten times bigger than $m_{\tilde{\chi}_1}$, and at the point of $m_{\tilde{\chi}_1} = 500$ GeV, $m_{\tilde{\chi}_2} = 5$ TeV, which is equal to $m_{\tilde{L}_2}$.

We further explore the dependence of $S_{\phi K_S}$ on the phase angle ϕ_L and the mixing angle θ_{23} in Fig. 3 and Fig. 4. We reduce the value of ϕ_L to 0.005 in Fig. 3. We continue to take $\tan\beta = 5$, $m_{\tilde{L}_2} = 5$ TeV and $m_{\tilde{\chi}_2} = 10 m_{\tilde{\chi}_1}$. As shown in the plot, with a smaller ϕ_L angle the allowed region is suppressed $m_{\tilde{L}_3} < 200$ GeV. In Fig. 4, θ_{23} is reduced to $\pi/6$ and ϕ_L is fixed to be 0.01. The allowed region changes as a result. Fig. 4 presents an even bigger change as θ decreases from $\pi/4$ to $\pi/6$.

There is one parameter left: $\tan\beta$, which is very important. From Eq. 12 and Eq. 15, we can see that $\tan\beta$ affects not only the mixing angles, but also the Wilson Coefficients. Any change in $\tan\beta$ alters $S_{\phi K_S}$ significantly. We plot Fig. 5 to explore the dependence of $S_{\phi K_S}$ on $\tan\beta$. Apart from $\tan\beta$, all the other parameters remain the same as the parameters in frame (a) of Fig. 2. In frame (a), we take $\tan\beta$ to be 20, while in frame (b), $\tan\beta$ is set to be 40. Several features are worth noting:

- By comparing two graphs in this figure, we find that the allowed region permits larger masses with the increase in $\tan\beta$.

- As for graph in frame (b), we just plot $S_{\phi K_S}$ in a region with the masses of $m_{\tilde{L}_3}$ and $m_{\tilde{\chi}_1}$ smaller than 1.5 TeV. There is a large allowed region beyond 1.5 TeV, which does not appear in this graph. Still, we can see the strong dependence of $S_{\phi K_S}$ on $\tan\beta$.

B. Right-Right Mixing Dominant

This corresponds to the case where left-left mixing is very small and can be ignored. The dominant mixing is right-right mixing. the mixing matrix is:

$$R = \begin{pmatrix} cos\theta_{56} & sin\theta_{56}e^{i\phi_R} \\ -sin\theta_{56} & cos\theta_{56}e^{-i\phi_R} \end{pmatrix}. \tag{19}$$

The free parameter are now

$$m_{\tilde{R}_2}, m_{\tilde{R}_3}, m_{\tilde{\chi}_2}, m_{\tilde{\chi}_1}, tan\beta, \theta_{56}, \phi_R.$$

with the same constraints $m_{\tilde{R}_3} < m_{\tilde{R}_2}$ and $m_{\tilde{\chi}_1} < m_{\tilde{\chi}_2}$.

Unlike the Left-Left dominant scenario, this time, we fix $m_{\tilde{R}_3} = 300$ GeV. In Fig. 6, we plot $S_{\phi K_S}$ as a function of $m_{\tilde{R}_2}$ and $m_{\tilde{\chi}_1}$. tanβ is still 5. We try different values of ϕ within the range $\phi \leq 0.01$, and find that in almost the whole range, the value of $S_{\phi K_S}$ is approximately 0.73, which is the same as the SM prediction. SUSY contributions are very small. We relax the ϕ constraint and take ϕ to be $\pi/4$. θ_{56} is also $\pi/4$. In frame (a), $m_{\tilde{\chi}_2} = 10 m_{\tilde{\chi}_1}$, while in frame (b), $m_{\tilde{\chi}_2}$ is 20 times bigger than $m_{\tilde{\chi}_1}$. From this graph, we notice that, in contrast to the left-left mixing case, the shaded region in frame (b) is concentrated toward small masses side than that in frame (a) . As shown in Eq. 12, the difference between the chargino masses, $m_{\tilde{\chi}_2} - m_{\tilde{\chi}_1}$ affects the mixing angles in the chargino sector. The mixing angles determine the values of $S_{\phi K_S}$. We allow $m_{\tilde{\chi}_2}$ to be proportional to $m_{\tilde{\chi}_1}$ such that the larger the mass of $m_{\tilde{\chi}_1}$, the bigger the mass difference of $m_{\tilde{\chi}_2}$ and $m_{\tilde{\chi}_1}$. It is the fact that $m_{\tilde{\chi}_2}$ in frame (b) is ten times bigger than the corresponding $m_{\tilde{\chi}_2}$ in frame (a) make the allowed $S_{\phi K_S}$ region in frame (a) concentrate on larger $m_{\tilde{\chi}_1}$, while in frame (b), $m_{\tilde{\chi}_1}$ is relatively small.

At $m_{\tilde{\chi}_1} = 300$ GeV, we observe a small peak in the graphs. As in the left-left mixing case, at this point $m_{\tilde{\chi}_1}$ equals to $m_{\tilde{R}_3}$, which uses a difference loop function.

We also wish to explore the dependence of $S_{\phi K_S}$ on other parameters. Unlike in left-left mixing case, this time instead of studying the dependence of $S_{\phi K_S}$ on each parameter, we show a graph scanning the whole parameter space:

$$m_{\tilde{L}_2}, m_{\tilde{L}_3}, m_{\tilde{\chi}_1}, m_{\tilde{\chi}_2}, \theta_{23}, \phi_R.$$

Within the constraints $m_{\tilde{R}_2} > m_{\tilde{R}_3}$ and $m_{\tilde{\chi}_2} > m_{\tilde{\chi}_1}$, we take:

$$\begin{aligned} 300\ GeV < m_{\tilde{R}2} < 2500\ GeV \\ 250\ GeV < m_{\tilde{R}3} < 1000\ GeV \\ 100\ GeV < m_{\tilde{\chi}_1} < 500\ GeV \\ 150\ GeV < m_{\tilde{\chi}_2} < 1000\ GeV \\ 0 < \theta_{23} < \pi/2 \\ 0 < \phi_R < 2\pi \end{aligned} \tag{20}$$

The results are present in Fig. 7 with $S_{\phi K_S}$ vs $m_{\tilde{\chi}_2}$. In frame (a), the tanβ is 15, and in frame (b) it is increased to 50. In frame (a), we notice that many of the points are around

0.73, the value of standard model prediction. This behavior tells us with the parameters in Eq. 20 SUSY contributions are usually small and cannot alter $S_{\phi K_S}$ substantially. What we are interested in is the regions of parameter space where SUSY contributions are dominant. In these regions, the value of $S_{\phi K_S}$ can be as low as negative -0.98. As tanβ increases, SUSY contributions are increased. As shown in frame (b), when tanβ is increased to 50, more points on the scatter plot deviate from the SM prediction. The mixing angles θ_U and θ_V in the chargino sector vary with tanβ and increase the SUSY contributions to $S_{\phi K_S}$. There are very few points within $m_{\tilde{\chi}_2} < 300$ GeV. That is because we require $m_{\tilde{\chi}_2} > m_{\tilde{\chi}_1}$, which limits the probability of small $m_{\tilde{\chi}_2}$.

C. Left-Left Mixing + Right-Right Mixing

Left-left mixing and right-right mixing are comparable in this scenario. They both make contributions to $S_{\phi K_S}$. There are two mixing angles, two phase angles and four mass parameters. To simplify the computation, we assume that left and right squarks have the same masses in same generation, that is: $m_{\tilde{L}_2} = m_{\tilde{R}_2} = \tilde{m}_2$ and $m_{\tilde{L}_3} = m_{\tilde{R}_3} = \tilde{m}_3$. With these assumptions, the mixing angles θ_L in the left-left mixing and θ_R in the right-right mixing are the same, $\theta_L = \theta_R = \theta$ and also the phase angle, $\phi_L = \phi_R = \phi$. Therefore, the free parameters in this scenario are reduced to:

$$\tilde{m}_2, \tilde{m}_3, m_{\tilde{\chi}_2}, m_{\tilde{\chi}_1}, tan\beta, \theta, \phi.$$

with the same constraints $\tilde{m}_3 < \tilde{m}_2$ and $m_{\tilde{\chi}_1} < m_{\tilde{\chi}_2}$.

We display our main results in a few plots. In Fig. 8, we fixed $\tilde{m}_2 = 5$ TeV and the mixing angle θ is set to be $\pi/4$. The phase angle ϕ is 0.01. In frame (a), we use $m_{\tilde{\chi}_2} = 10 m_{\tilde{\chi}_1}$, while in frame (b) $m_{\tilde{\chi}_2}$ is 50 times bigger than $m_{\tilde{\chi}_1}$. This graph is very similar to the corresponding graph in left-left mixing scenario, Fig 2, except here we have a larger allowed parameter space. As in the LL dominant scenario, chargino masses affect $S_{\phi K_S}$ significantly. This is shown in the difference between graphs in frame (a) and frame (b). As expected, left-left mixing provides the dominant contribution and right-right mixing adds to the allowed region. The big gaps around line $\tilde{m}_3 = m_{\tilde{\chi}_1}$ and the small gap at $\tilde{m}_2 = m_{\tilde{\chi}_2}$ are much more obvious than in left-left dominant scenario. We can conclude that left-left plus right-right mixing together make a big contribution to $S_{\phi K_S}$.

$S_{\phi K_S}$ also depends on the mixing and phase angles. Fig. 9 shows the effect of phase angle ϕ, while Fig. 10 shows the effect of the mixing angle θ. We keep $\tilde{m}_2 = 5$ TeV and $m_{\tilde{\chi}_2} = 10 m_{\tilde{\chi}_1}$. In Fig. 9, the phase angle ϕ is reduced to 0.005 and mixing angle is fixed to be $\pi/4$, while in Fig. 10, θ changes to $\pi/6$ and ϕ is kept at 0.01. As in the LL case, as ϕ decreases the allowed parameter space decreases and as θ becomes smaller the allowed masses also become smaller.

Fig. 11 is the scanned graph. We scan the same parameter space as in the right-right mixing case. We find that in frame (a), although there is still a concentration of points around the standard model value, more points deviate from their SM prediction than with only right-right mixing. This effect is even more obvious in frame (b). This also shows a stronger contribution in this scenario.

IV. CONCLUSION

We have studied the supersymmetric contributions, especially the chargino loop contributions, to CP asymmetry in $B \to \phi K_S$ decay. To emphasize chargino loop contributions, we work in a special basis where the down-type squark mass matrix is diagonal. In this special basis, gluino loop contributions, which are very important in most SUSY frames, are ruled out. Chargino loops are the main contributions to $S_{\phi K_S}$.

Within the allowed parameter region, we studied three special cases. Left-left mixing dominant, right-right mixing dominant and left-left plus right-right mixing dominant. In the LL case, chargino contributions to the CP asymmetry can be much larger than the SM contributions in some regions of parameter space. The CP asymmetry $S_{\phi K_S}$ varies significantly as the chargino masses vary. In the RR case, things are very similar with the LL case, except the allowed region is totally different from the LL case. The LL plus RR mixing gives the largest contribution to $S_{\phi K_S}$.

We consider SUSY contributions to CP asymmetry $S_{\phi K_S}$ with only chargino loops. In most SUSY scenarios, gluino loops will provide very large contributions, which may be larger than chargino contributions for some parameters. Gluino, chargino and even neutralino loops make up the whole SUSY contribution.

$b \to s\gamma$ decay puts very strong limits on the allowed parameter space. It excludes some regions in our graphs. The calculation of $b \to s\gamma$ is very model dependent. We are not including the $b \to s\gamma$ constraints in our paper. But we can still conclude that SUSY is a candidate to explain the CP asymmetry deviation in $B \to \phi K_S$ and $B \to J/\psi K_S$ and the contributions of chargino loops play an important role in some regions of SUSY parameter space.

ACKNOWLEDGMENTS

It is a pleasure to thank Professor G. Valencia for his helpful comments and valuable information in the loop function computation. Thanks Professor D. Atwood for the discussion on this paper. Thanks Dr. J. Abraham to help me editing this paper. This research was supported in part by the U.S. Department of Energy under contracts number DE-FG02-01ER41155

APPENDIX A: LOOP FUNCTIONS

$$
\begin{aligned}
G(A,B,C) &= \int_0^\infty \frac{z^2\,dz}{(z+1)(z+A)(z+B)(z+C)} \\
&= \frac{A^2\log A}{(A-1)(A-B)(A-C)} + \frac{B^2\log B}{(B-1)(B-A)(B-C)} \\
&\quad + \frac{C^2\log C}{(C-1)(C-A)(C-B)}, \qquad \text{(A1)} \\
G1(A,B,C) &= \int_0^\infty \frac{z\,dz}{(z+1)(z+A)(z+B)(z+C)}
\end{aligned}
$$

$$= -\frac{A\log A}{(A-1)(A-B)(A-C)} - \frac{B\log B}{(B-1)(B-A)(B-C)} - \frac{C\log C}{(C-1)(C-A)(C-B)}, \tag{A2}$$

$$C_1(x) = \frac{2x^3 - 9x^2 + 18x - 11 - 6\log x}{36(1-x)^4}, \tag{A3}$$

$$C_2(x) = \frac{-16x^3 + 45x^2 - 36x + 7 + 6x^2(2x-3)\log x}{36(1-x)^4}, \tag{A4}$$

$$D_1(x) = \frac{-x^3 + 6x^2 - 3x - 2 - 6x\log x}{6(1-x)^4}, \tag{A5}$$

$$D_2(x) = \frac{-x^2 + 1 + 2x\log x}{(x-1)^3}, \tag{A6}$$

REFERENCES

[1] N. Cabibbo, Phys. Rev. Lett.**10**, 531(1963); M. Kobayashi and K. Maskawa, Prog. Theor. Phys. **49**, 652(1973).
[2] B. Aubert et al. (BABAR Collaboration), Phys. Rev. Lett. **89** (2002) 201802.
[3] K. Abe et al. (Belle Collaboration), Phys. Rev. **D66**, 71102(2002).
[4] Y. Nir, Nucl.Phys.Proc.Suppl.**117**,111(2003).
[5] R. Fleischer and T. Mannel, Phys. Lett. **B511**, 240(2001).
[6] C.W. Chiang and J.L. Rosner, Phys. Rev. **D68**, 14007(2003)
[7] J. Rosner, *Introduction to B Physics.* hep-ph/0304200.
[8] T. Hurth and E. Lunghi, hep-ph/0307142.
[9] D. Atwood and G. Hiller, hep-ph/0307251.
[10] E. Gabrielli and G. Giudice, Nucl. Phys. **B433**,3(1994), Erratum-ibid, **B507**, 549(1997).
[11] A. Datta, Phys. Rev. **D66**, 71702(2002).
[12] A. M. Teixeira, hep-ph/0209129.
[13] J. Lee and K. Lee, Eur. Phys. J. **C29**, 373(2003).
[14] A. Kundu and T. Mitra, Phys. Rev. **D67**, 116005(2003).
[15] K. Agashe and C. D. Carone, hep-ph/0304229.
[16] J. Cheng, C. Huang and X. Wu, hep-ph/0306086.
[17] R. Arnowitt, B. Dutta and B. Hu, hep-ph/0307152.
[18] C. Dariescu, M. Dariescu, N. Deshpande and D. Ghosh, hep-ph/0308305.
[19] F. Gabbiani and A. Masiero, Nucl. Phys. **B322**, 235(1989); F. Gabbiani, E. Gabrielli, A. Masiero and L. Silvestrini, Nucl. Phys. **B477**, 321(1996).
[20] T. Moroi, Phys. Lett. **B493**, 366(2000).
[21] E. Lunghi and D. Wyler, Phys. Lett. **B521**, 320(2001).
[22] S. Khalil and E. Kou, Phys. Rev. **D67**, 55009(2003).
[23] R. Harnik, D. Larson, H. Murayama and A. Pierce, hep-ph/0212180.
[24] G. L. Kane, P. Ko, H. wang, C. Kolda, J. Park and L. Wang, Phys. Rev. Lett. **90**, 141803(2003).
[25] D. Chakraverty, E. Gabrielli, K. Huitu and S. Khalil, hep-ph/0306076.
[26] G. Branco, P. Parada and M. Rebelo, hep-ph/0307119.
[27] Y. Grossman and M. Worah, Phys. Lett. **B395**, 241(1997).
[28] S. Mishima, Phys. Lett. **B521**, 252(2001); S. Mishima and A. Sanda, Prog. Theor. Phys. **110**, 549(2003).
[29] C. Bobeth, T. Ewerth, F. Krüger and J. Urban, Phys. Rev. D **64**, 074014 (2001).
[30] G. Buchalla, A. J. Buras and M. Lautenbacher, Rev. Mod. Phys. **68**, 1125 (1996).
[31] H. E. Haber and G. L. Kane, Phys.Rept.**117**, 75(1985);
[32] S. Bertolini, F. Borzumati and A. Masiero, Nucl. Phys. **B294**, 321(1987); S. Bertolini, F. Borzumati, A. Masiero and G. Ridolfi, Nucl. Phys. **B353**, 591(1991).
[33] F. Krüger and J. C. Romão, Phys. Rev. **D62**, 34020(200).
[34] R. Barbieri and A. Strumia, Nucl. Phys. **B508**,3(1997).
[35] E. Gabrielli and S. Khalil, Phys. Rev. **D67**, 15008(2003).

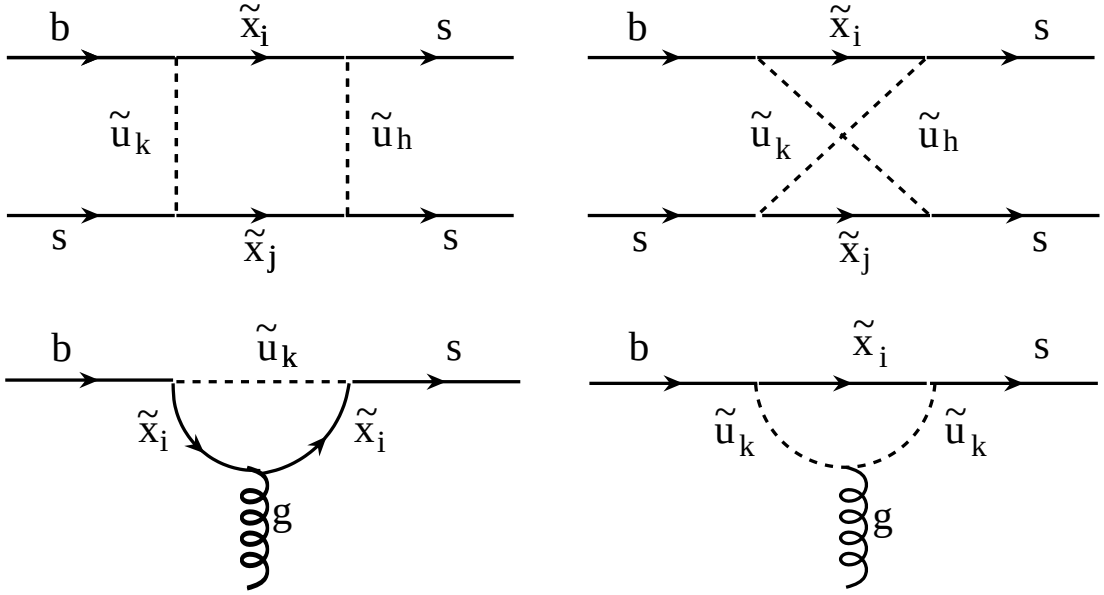

FIG. 1. Box and penguin diagrams in $b \to s\bar{s}s$.

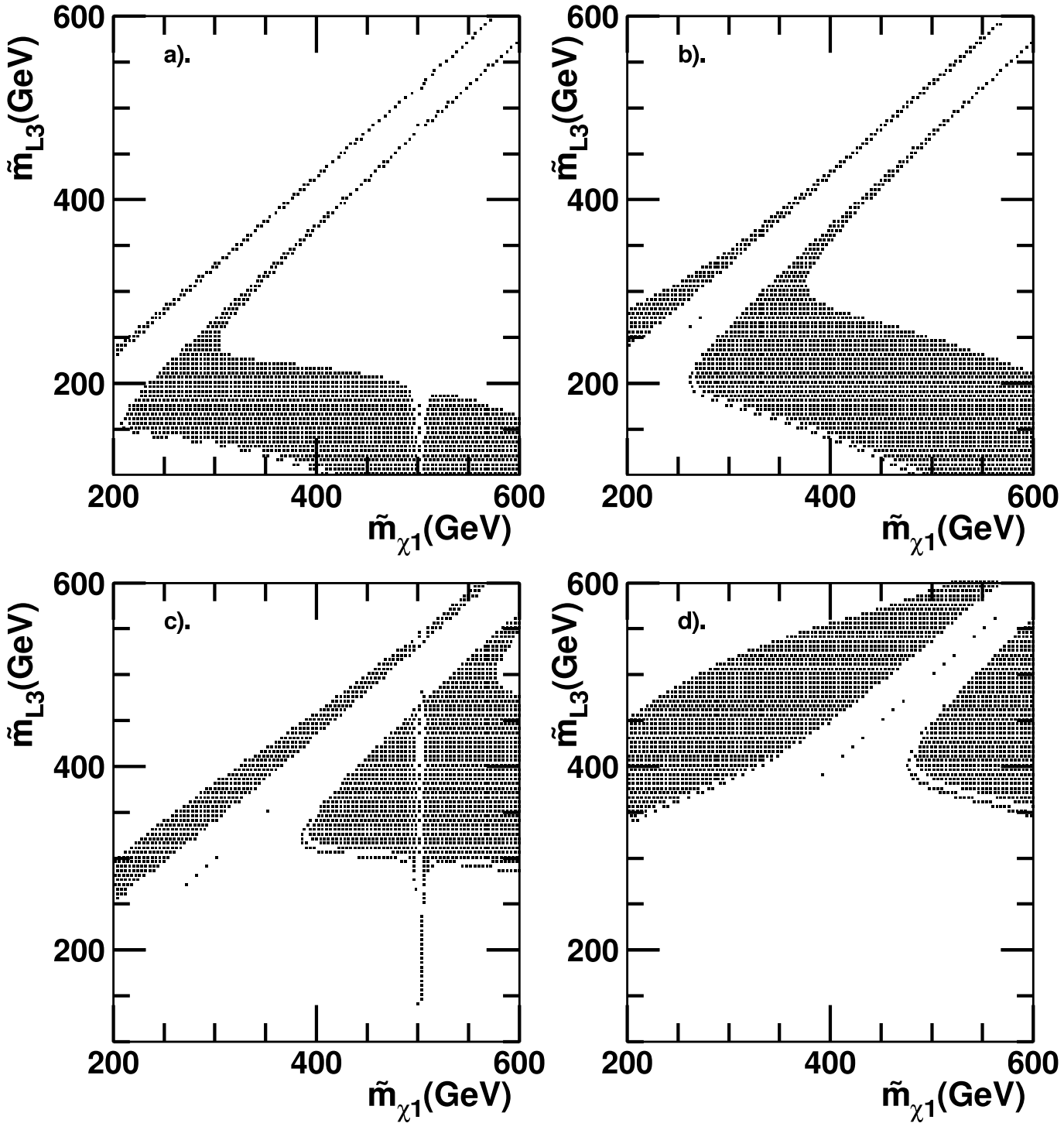

FIG. 2. In left-left mixing scenario, $S_{\phi K_S}$ in the plane of $\tilde{m}_{L3}$ vs $\tilde{m}_{\chi_1}$. The shaded region corresponds to $-0.7 < S_{\phi K_S} < 0.7$ with $\phi = 0.01$ and $\theta = \pi/4$. (a). $\kappa = -1.1$, $\tilde{m}_{\chi 2} = 10\tilde{m}_{\chi 1}$; (b). $\kappa = -1.1$, $\tilde{m}_{\chi 2} = 100\tilde{m}_{\chi 1}$; (c). $\kappa = -2.$, $\tilde{m}_{\chi 2} = 10\tilde{m}_{\chi 1}$; (d). $\kappa = -2.$, $\tilde{m}_{\chi 2} = 100\tilde{m}_{\chi 1}$;

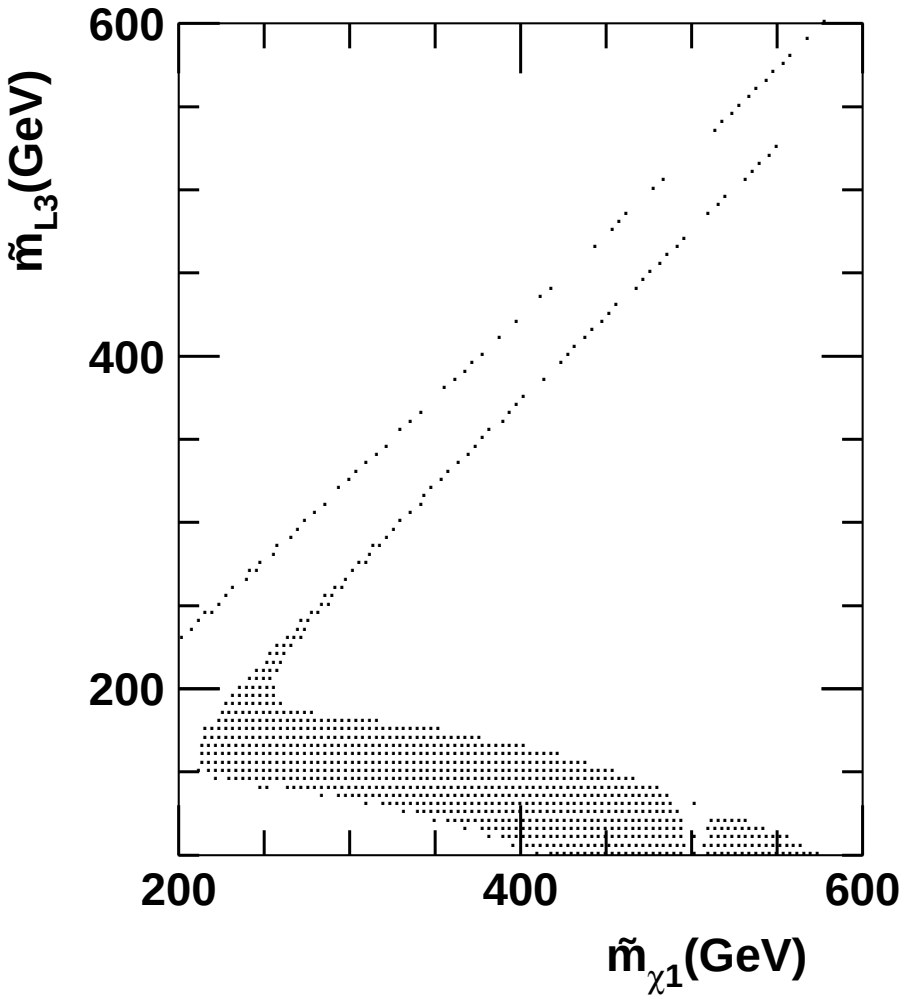

FIG. 3. In left-left mixing scenario, $S_{\phi K_S}$ in the plane of $\tilde{m}_{L3}$ vs $\tilde{m}_{\chi_1}$. The shaded region corresponds to $-0.7 < S_{\phi K_S} < 0.7$ with $\phi = 0.005$, $\theta = \pi/4$ and $\kappa = -1.1$. $\tilde{m}_{\chi 2} = 10\tilde{m}_{\chi 1}$

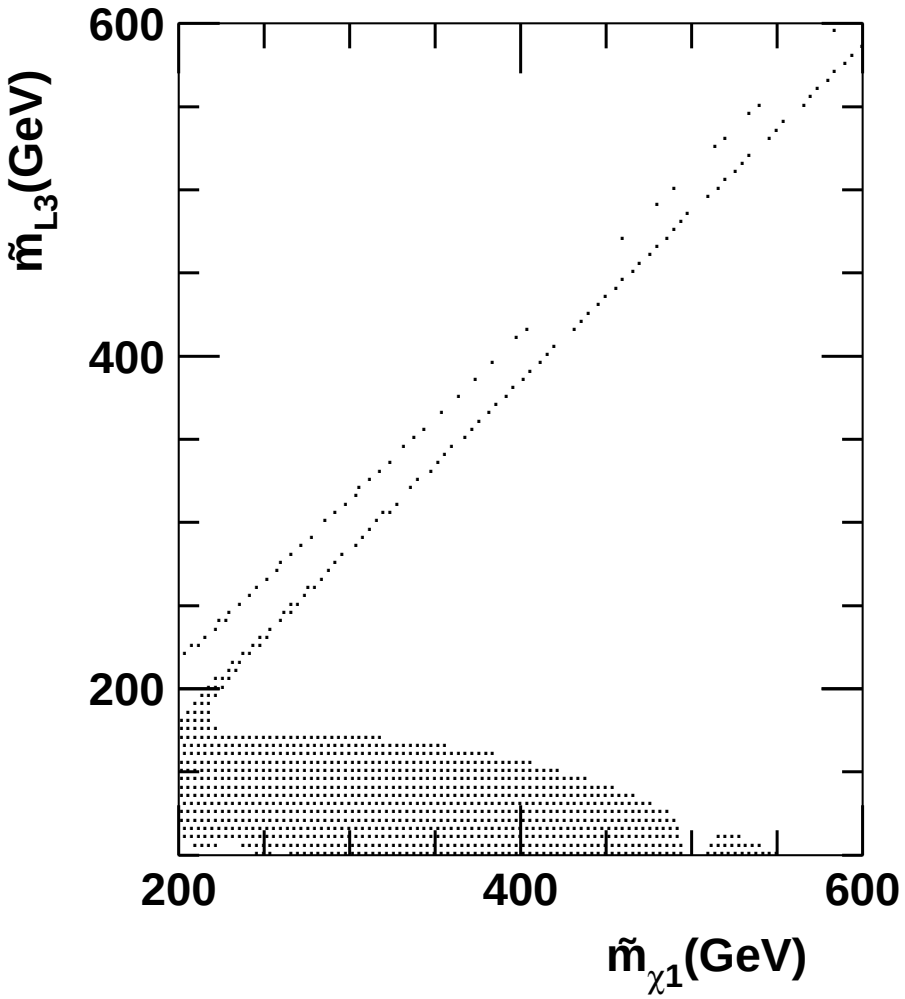

FIG. 4. In left-left mixing scenario, $S_{\phi K_S}$ in the plane of $\tilde{m}_{L3}$ vs $\tilde{m}_{\chi_1}$. The shaded region corresponds to $-0.7 < S_{\phi K_S} < 0.7$ with $\phi = 0.01$, $\theta = \pi/6$ and $\kappa = -1.1$. $\tilde{m}_{\chi 2} = 10\tilde{m}_{\chi 1}$

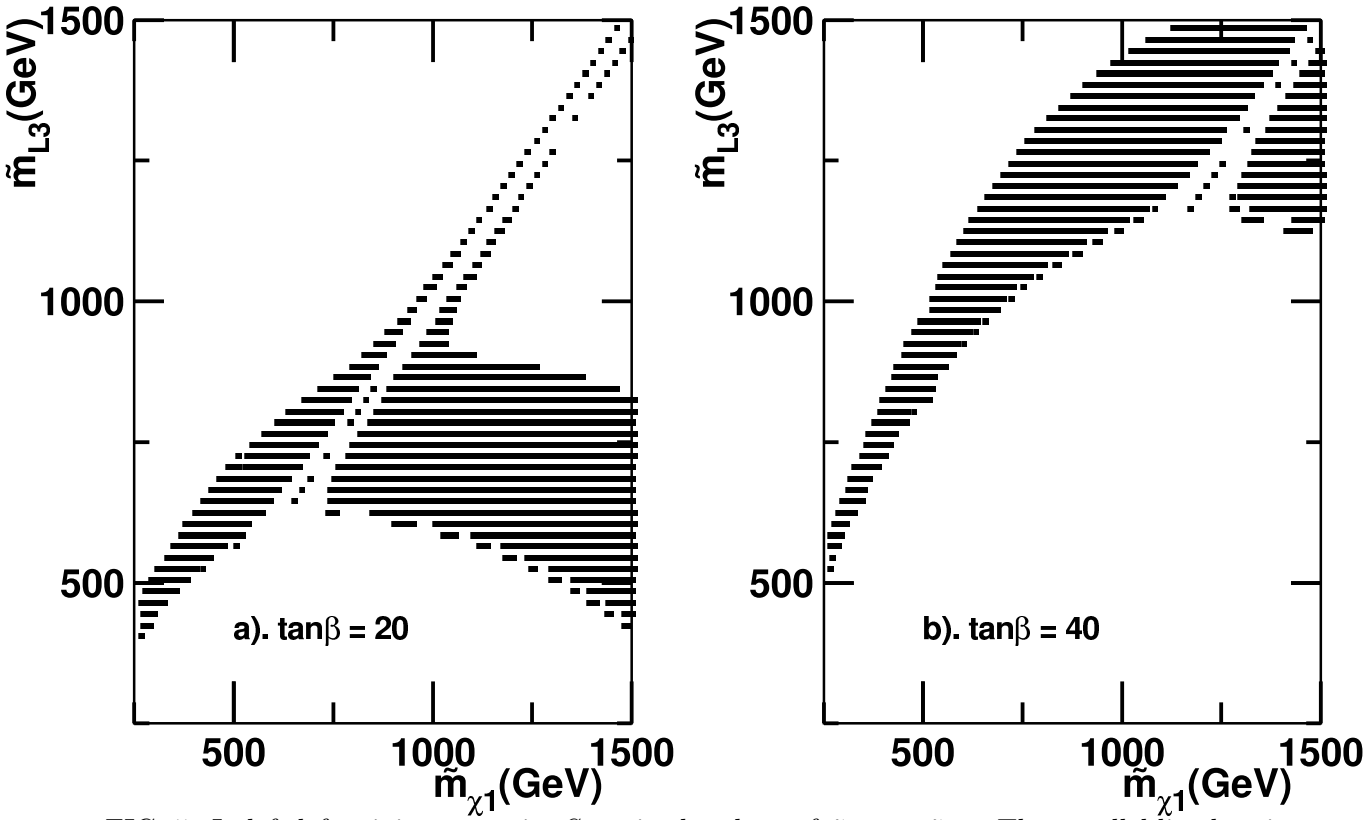

FIG. 5. In left-left mixing scenario, $S_{\phi K_S}$ in the plane of $\tilde{m}_{L3}$ vs $\tilde{m}_{\chi_1}$. The parallel lined region corresponds to $-0.7 < S_{\phi K_S} < 0.7$ with $\phi = 0.01$, $\theta = \pi/4$ and $\kappa = -1.1$. $\tilde{m}_{\chi 2} = 10\tilde{m}_{\chi 1}$. (a) tan$\beta$ = 20; (b) tanβ = 40.

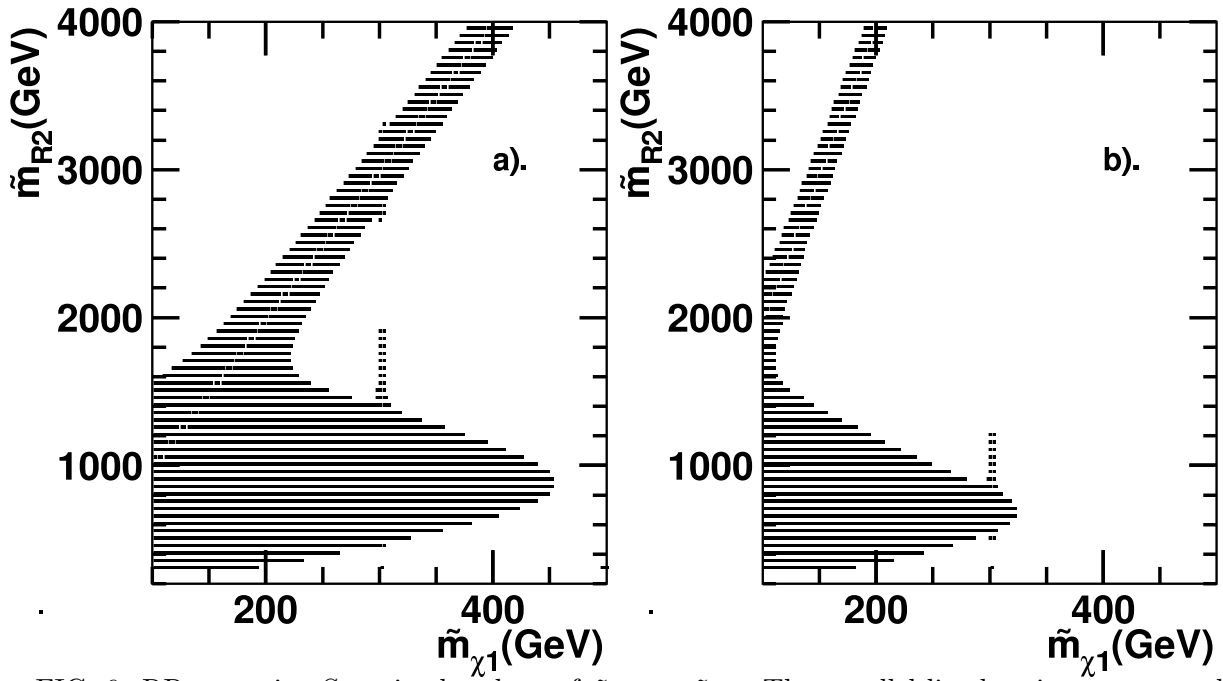

FIG. 6. RR scenario. $S_{\phi K_S}$ in the plane of $\tilde{m}_{L3}$ vs $\tilde{m}_{\chi_1}$. The parallel lined region corresponds to $-0.7 < S_{\phi K_S} < 0.7$ with $\phi = \pi/4$, $\theta = \pi/4$ and $\kappa = -1.1$. (a) $\tilde{m}_{\chi 2} = 10\tilde{m}_{\chi 1}$; (b) $\tilde{m}_{\chi 2} = 100\tilde{m}_{\chi 1}$;

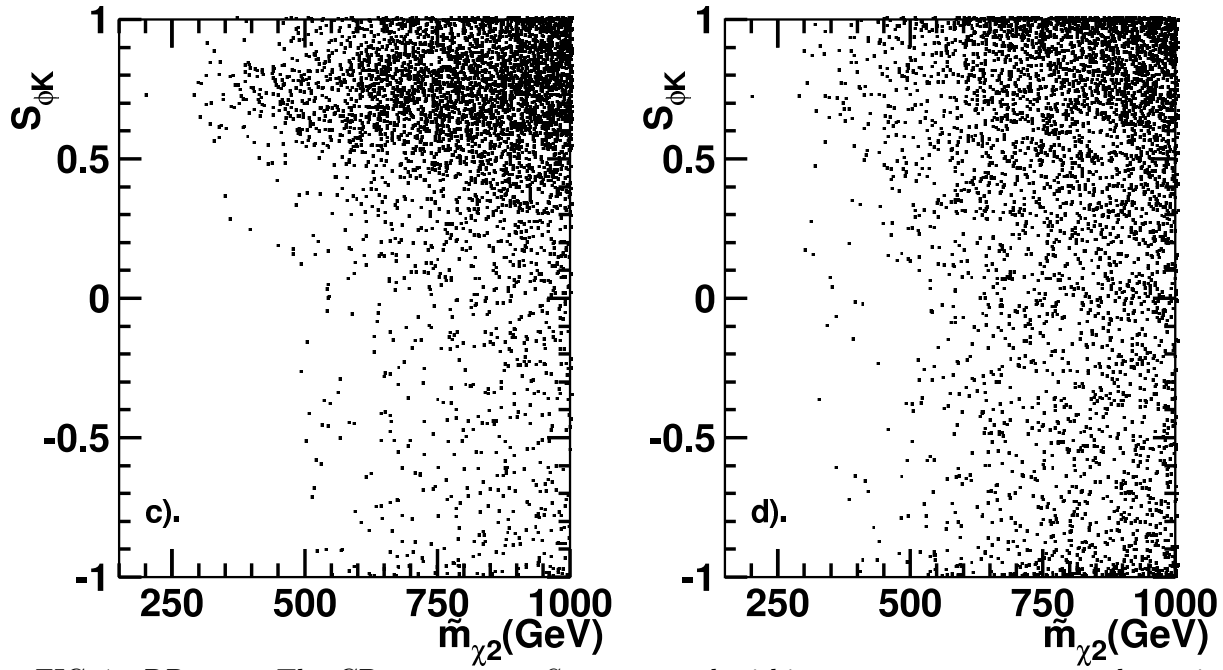

FIG. 7. RR case. The CP asymmetry $S_{\phi K_S}$ scanned within parameter space over the region mentioned in the text. We show the results in the plane of $S_{\phi K_S}$ vs $\tilde{m}_{L3}$ with (a). $\tan\beta = 15$ and (b). $\tan\beta = 50$

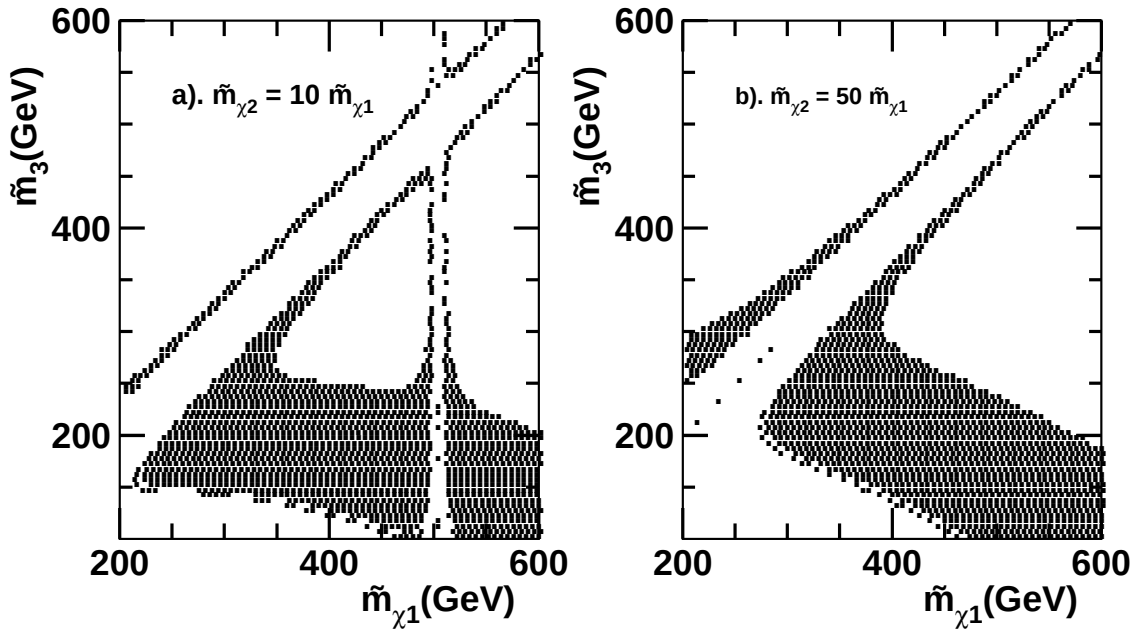

FIG. 8. In LL + RR mixing case. $S_{\phi K_S}$ in the plane of $\tilde{m}_{L3}$ vs $\tilde{m}_{\chi_1}$. The shaded region corresponds to $-0.7 < S_{\phi K_S} < 0.7$ with $\phi = 0.01$, $\theta = \pi/4$ and $\kappa = -1.1$. (a) $\tilde{m}_{\chi 2} = 10\tilde{m}_{\chi 1}$; (b) $\tilde{m}_{\chi 2} = 50\tilde{m}_{\chi 1}$;

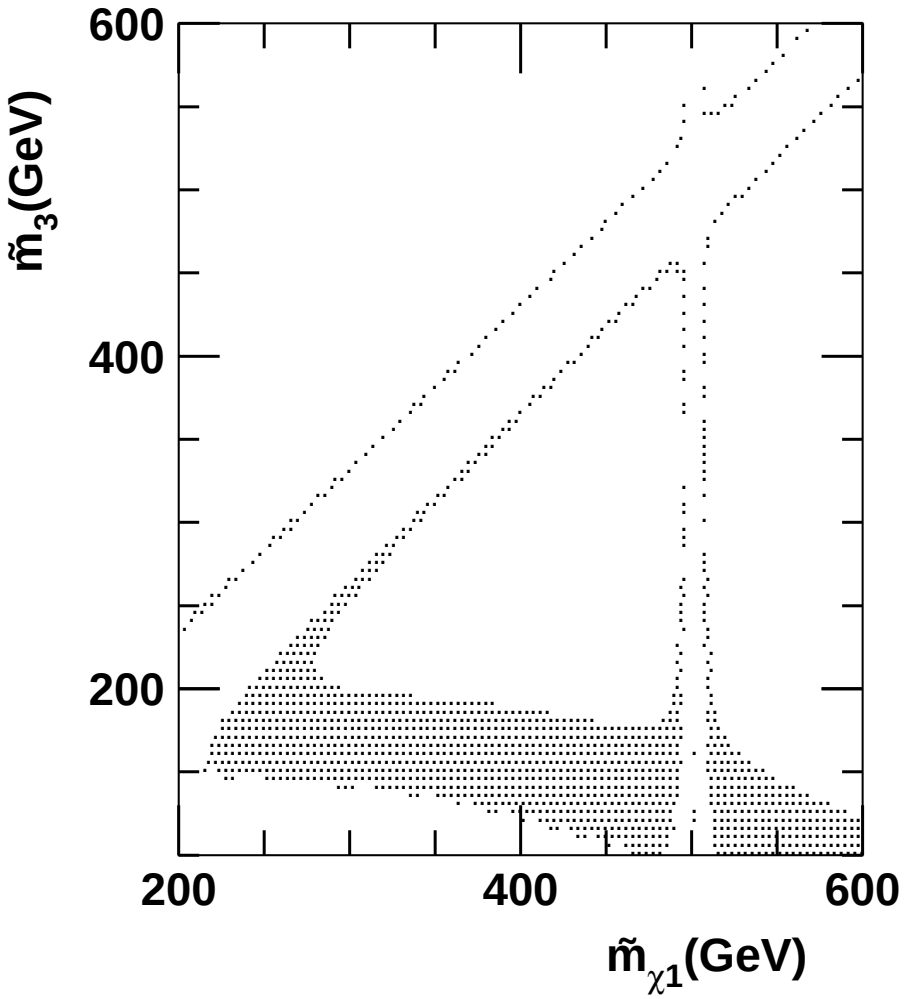

FIG. 9. LL + RR case. $S_{\phi K_S}$ in the plane of $\tilde{m}_{L3}$ vs $\tilde{m}_{\chi_1}$. The shaded region corresponds to $-0.7 < S_{\phi K_S} < 0.7$ with $\phi = 0.005$, $\theta = \pi/4$ and $\kappa = -1.1$. $\tilde{m}_{\chi 2} = 10\tilde{m}_{\chi 1}$

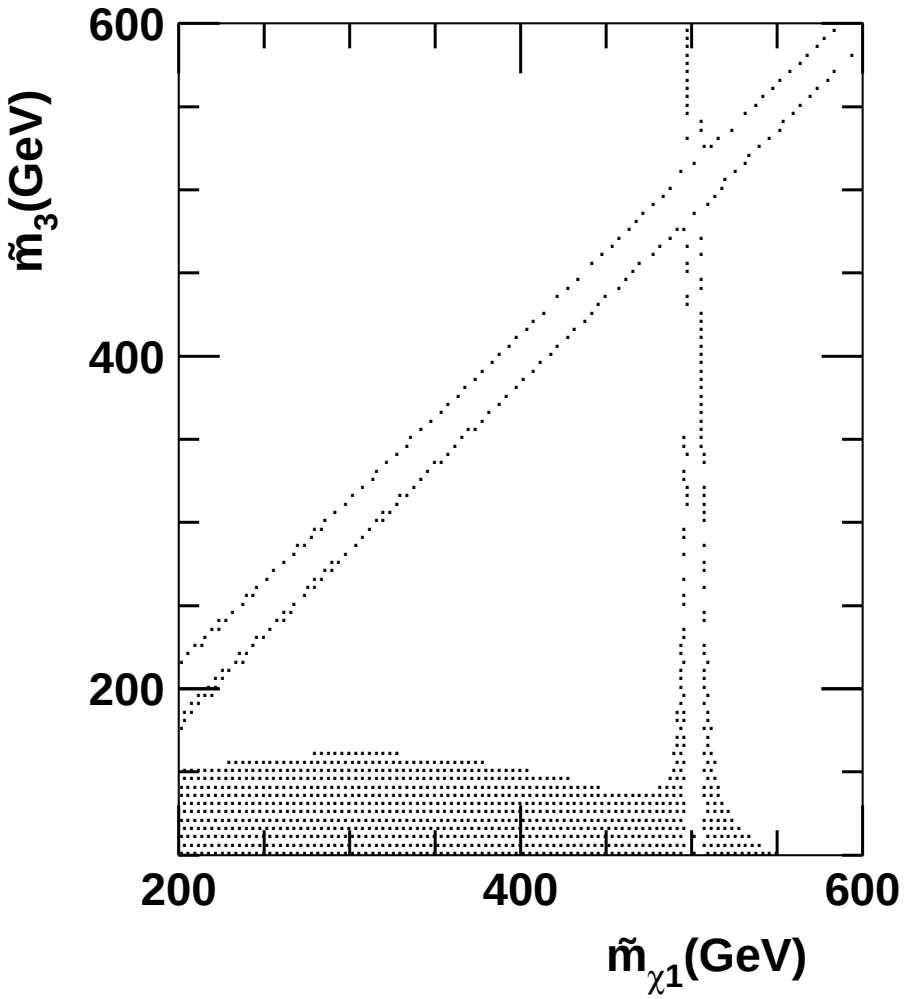

FIG. 10. LL + RR case. $S_{\phi K_S}$ in the plane of $\tilde{m}_{L3}$ vs $\tilde{m}_{\chi_1}$. The shaded region corresponds to $-0.7 < S_{\phi K_S} < 0.7$ with $\phi = 0.01$, $\theta = \pi/6$ and $\kappa = -1.1$. $\tilde{m}_{\chi 2} = 10\tilde{m}_{\chi 1}$

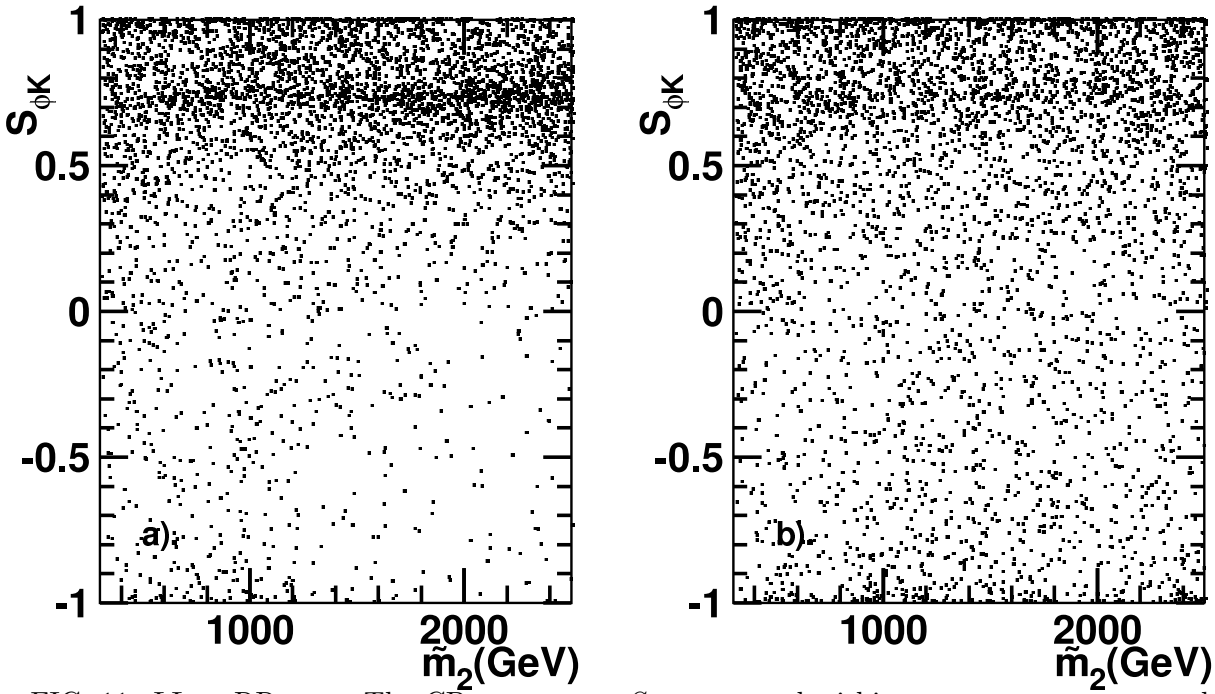

FIG. 11. LL + RR case. The CP asymmetry $S_{\phi K_S}$ scanned within parameter space over the region mentioned in the text. We show the results in the plane of $S_{\phi K_S}$ vs $\tilde{m}_{L3}$ with (a). tanβ = 15 and (b). tanβ = 50